Low-frequency percolation scaling for particle diffusion in electrostatic turbulence

J.-D. Reuss* and J. H. Misguich†
Association Euratom Commissariat à I'Energie Atomique sur la Fusion, DRFC, Centre d'Etudes de Cadarache, F-13108 Saint-Paul-lez-Durance Cedex, France
(Received 23 February 1996)

An important point for turbulent transport consists in determining the scaling law for the diffusion coefficient D due to electrostatic turbulence as a function of the control parameter $A \approx E/\omega B$ proportional to the ratio of the rms electric field to the magnetic field strength times an average frequency ω. It is well known that for weak amplitudes or large frequencies, the reduced diffusion coefficient $\mathbb{D} \approx D/\omega \approx A^{\gamma}$ has a quasilinearlike (or gyro-Bohm-like) scaling ($\gamma=2$), while for large amplitudes or small frequencies it has been traditionally believed that the scaling is Bohm-like ($\gamma=1$). Only recently a percolation critical exponent ($\gamma=\frac{7}{10}$) has been predicted by Isichenko. The aim of this work consists of testing this prediction for a given realistic model. This problem is studied here by direct simulation of particle trajectories. Guiding center diffusion in a spectrum of electrostatic turbulence is computed for test particles in a model spectrum, by means of a new parallelized code RADIGUET 2 described here. The spectrum involves only one frequency ω but a large number of randomly phased electrostatic plane waves, propagating isotropically in the plane perpendicular to the confining strong magnetic field. This ensures chaotic trajectories. This set of waves represents standing waves. Their amplitudes depend on wavelength in order to reproduce the k^{-3} domain of the observed spectrum in tokamaks. The results indicate a continuous transition for large amplitudes toward a value of $\gamma=0.704\pm0.030$ which is compatible with the Isichenko percolation prediction. [S1063-651X(96)01907-1]

PACS number(s): 52.25.Fi, 52.34.Ra, 52.65.Cc

I. INTRODUCTION

Scaling properties for transport laws in hot magnetized plasmas are presently of huge interest in thermonuclear fusion research, especially in the perspective of building future large tokamaks such as the ITER (International Thermonuclear Experimental Reactor) project. Although much progress has been achieved recently, a detailed understanding of the actual mechanisms responsible for the observed ''anomalous transport'' is far from being reached. The most probable candidates are, of course, electric and magnetic fluctuations occurring spontaneously in the plasma, but also nonlocal transport and self-organization of the plasma.

Here we focus our attention on the local transport properties of test particles in a given spectrum of electrostatic turbulence, i.e., without trying to determine this spectrum in a self-consistent way. Electrostatic fluctuations have been measured in tokamak plasmas [1] and the wave number spectrum is well known, involving a k^{-3} power-law subrange [1,2]. It thus seems interesting to study transport properties for test particles in such a turbulent spectrum.

Theoretical predictions for the scaling properties of the diffusion coefficient of test guiding centers in an electrostatic turbulence are actually very old. Almost 30 years ago, Dupree [3] derived, in the domain of low frequencies, a very nice result from his renormalized turbulence theory (second cumulant and Corrsin approximation). He found that in this limit the well-known Bohm scaling [4] is recovered for the diffusion coefficient as a function of the magnetic field strength $D \approx B^{-\gamma}$ with

$$\gamma_B = 1. \tag{1.1}$$

More precisely, we have $D \approx \omega k_*^{-2} A^{+\gamma}$ as a function of the dimensionless amplitude $A \approx c k_* E/\omega B$ [see Eq. (2.28)], where k_* and ω are the typical wave vector and frequency in the turbulent spectrum. The same conclusion has been reached for a very different model by Taylor and McNamara [5], and also by Montgomery [6].

From a nonlinear treatment of the guiding center equations, we have derived a general equation describing particle diffusion in a general spectrum with two different power-law ranges and we recovered the Bohm scaling in the limit of high amplitudes or frozen turbulence [7]. The numerical solution actually shows for increasing amplitudes a continuous transition from a quasilinear scaling ($\gamma_{\mathrm{QL}}=2$) to a Bohm scaling [8]. In previous simulations by Misguich and coworkers [8–11], the high-amplitude results have always been interpreted traditionally as compatible with a Bohm scaling.

We know today that these predictions cannot be true: the simple reason has been given in Ref. [12], and is summarized in Sec. II [Eq. (2.34)]. Actually, in the limit of frozen turbulence, a percolation mechanism has been invoked by Isichenko and co-workers [12–15], which results in a prediction for the diffusion scaling at high amplitude or low frequencies:

$$\gamma_I = \tfrac{7}{10}. \tag{1.2}$$

This result appears as a critical exponent for this problem and should be an exact number. The result (1.2) appears in Isichenko's description as the combination $\gamma_I = 1-(\mu+d-3)/(d+1/\nu)$, where μ and d characterize the *static equipotentials* (which are the trajectories at zero frequency), while ν characterizes the *particle dynamics* at

*Electronic address: reuss@drfc.cad.cea.fr
†Electronic address: misguich@drfc.cad.cea.fr

finite frequency. The exponent $\mu=2$ describes the probability $p(s)\simeq s^{-\mu}$ of occurrence of equipotentials of size s, while the exponent $d=\frac{7}{4}$ measures the length $L(s)\simeq s^{d}$ of closed *fractal equipotentials* of size s. We do not discuss here this rather idealized description, nor its precise applicability to the present model. Such discussions are left for future work.

The aim of the present work consists of building a numerical code for the parallel computer Cray T3D in order to test this last prediction in the presence of a large number of waves. It will be checked that it is indeed verified within the uncertainty bars, in a domain of large amplitudes.

An important question remains: what is the reason for the general failure of these various Bohm predictions for the value of γ? The mathematical explanation for the appearance in frozen turbulence of this Bohm scaling law has been given in Ref. [7] in the context of the so-called Dupree-Weintock approximation. The latter is known [16] to involve a Gaussian-like approximation, along with the Corrsin factorization approximation [17,18]. Actually it has already been verified that for long times the diffusion process becomes Gaussian [19], as expected [20]. For this reason one can think that it is actually the Corrsin factorization approximation which could fail in the domain of large amplitudes because of the occurrence in the observed trajectories of long quasitrapping events interrupted by long jumps responsible for the final diffusion. This would surely be the most important qualitative conclusion from the present numerical work.

Our present result, which holds in the presence of a very large number of electrostatic waves, does not agree with a previous attempt to verify the percolation scaling (1.2). In a nice simulation work, Ottaviani [19] has considered an ensemble of only 64 electrostatic waves, but with stochastic amplitudes varying in time. He has only confirmed the general trend of the result

$$1-\gamma_O=+0.2\pm0.04 \tag{1.3}$$

but the percolation prediction (1.2) would rather give $1-\gamma_I=\frac{3}{10}$. The Ottaviani result (1.3), with the given error bar, thus excludes the possibility of a percolation scaling in this system. It thus seems to be useful to test the Isichenko prediction with a large number of wave vectors.

In Sec. II we present the physical content of the code RADIGUET 2. We discuss successively the model potential in Sec. II A, along with the average and fluctuating energy density (Sec. II B). The dimensionless equations of motion derived in Sec. II C involve four spatial cartographies of static electric field components, with periodic time variation. The physical meanings of the numerical parameters are discussed in Sec. II D. In Sec. III we present the structure and the numerical algorithms involved in our code RADIGUET 2. The results are discussed in Sec. IV.

II. EQUATIONS OF MOTION

We describe guiding center motion in a constant and static magnetic field $\mathbf{B}$ in the presence of a fluctuating electric field $\mathbf{E}(\mathbf{x},t)$ by the drift equation

$$\frac{d}{dt}\,\mathbf{x}(t)=\frac{c}{B^2}\,[\mathbf{E}(x(t),t)\times\mathbf{B}]. \tag{2.1}$$

The magnetic field is considered to be constant and uniform, in the z direction, and the electrostatic waves are propagating isotropically in the perpendicular plane. This equation is essentially nonlinear and allows for chaotic motion as soon as there are more than two phase velocities [21,22]. A randomly phased realization of the electrostatic field has to be built analytically such that it corresponds to a k^{-3} spectrum, where $\mathbf{k}$ is the wave vector in the plane perpendicular to the z axis.

A. Choice of the model potential

The spectrum of measured fluctuations in tokamak plasmas [1] involves a k^{-3} power-law subrange, already discussed in [23,24], which is very near the prediction $k^{-17/6}$ developed in [25] or the prediction $k^{-10/3}$ of the renormalized theory developed in [26]. This is the spectrum we are studying here, in a wave-vector domain limited by $(k_{\min},k_{\max})$.

The model described here is derived from a preliminary model we have presented in [8] and published in [9]. We later presented a more realistic model in [10], which remains isotropic in the plane perpendicular to z, in agreement with experimental observations [2]. The results for particle diffusion in this model have been obtained by means of a first vectorized code RADIGUET (Relative and Absolute Diffusion in GUiding center Electrostatic Turbulence) and were published in [11].

The discretization of the problem is performed as follows. The k^{-3} spectrum is obtained by building the electrostatic potential $\Phi(x,y,t)$ as a sum of discrete plane waves, with amplitudes $a_{\mathbf{k}}$ and frequency ω,

$$\Phi(x,y,t)\simeq\sum_{\mathbf{k}}\,a_{\mathbf{k}}\cos[\mathbf{k}\cdot\mathbf{x}-\omega t+\varphi_{\mathbf{k}}]. \tag{2.2}$$

The wave vectors $\mathbf{k}=(k_x,k_y)$ are distributed isotropically in the plane perpendicular to the magnetic field, and random phases $\varphi_{\mathbf{k}}$ associated to each wave. Due to isotropy, this represents a set of standing waves. An example of equipotential curves is given in Fig. 1.

This potential (2.2) is defined on a square of side L, supposed to be periodic in the plane (x,y). The components of the wave vectors are thus integer multiples of the elementary discretization wave vector $k_0=2\pi/L$ and are represented by the wave numbers m and n:

$$\mathbf{k}=\frac{2\pi}{L}\begin{pmatrix}n\\ m\end{pmatrix}. \tag{2.3}$$

The spectral domain $(k_{\min},k_{\max})$ is thus determined in the (k_x,k_y) plane by a circular annulus $C(N_0,N)$ limited by the radii $k_{\min}\equiv N_0k_0$ and $k_{\max}=Nk_0$. For instance, a spectral domain of width $k_{\max}/k_{\min}=12$ can be represented by using $N_0=4$ and $N=48$, which determines in the annulus a set of 7168 couples of integer values for (n,m), thus 7168 plane waves (the simple case $N_0=4$ and $N=9$ is shown in Fig. 2).

The size L of the periodic box is related to the discretization vector by $L=2\pi/k_0$. It is also related to the characteristic wavelengths

$$L=N_0\lambda_{\max}=N\lambda_{\min} \tag{2.4}$$

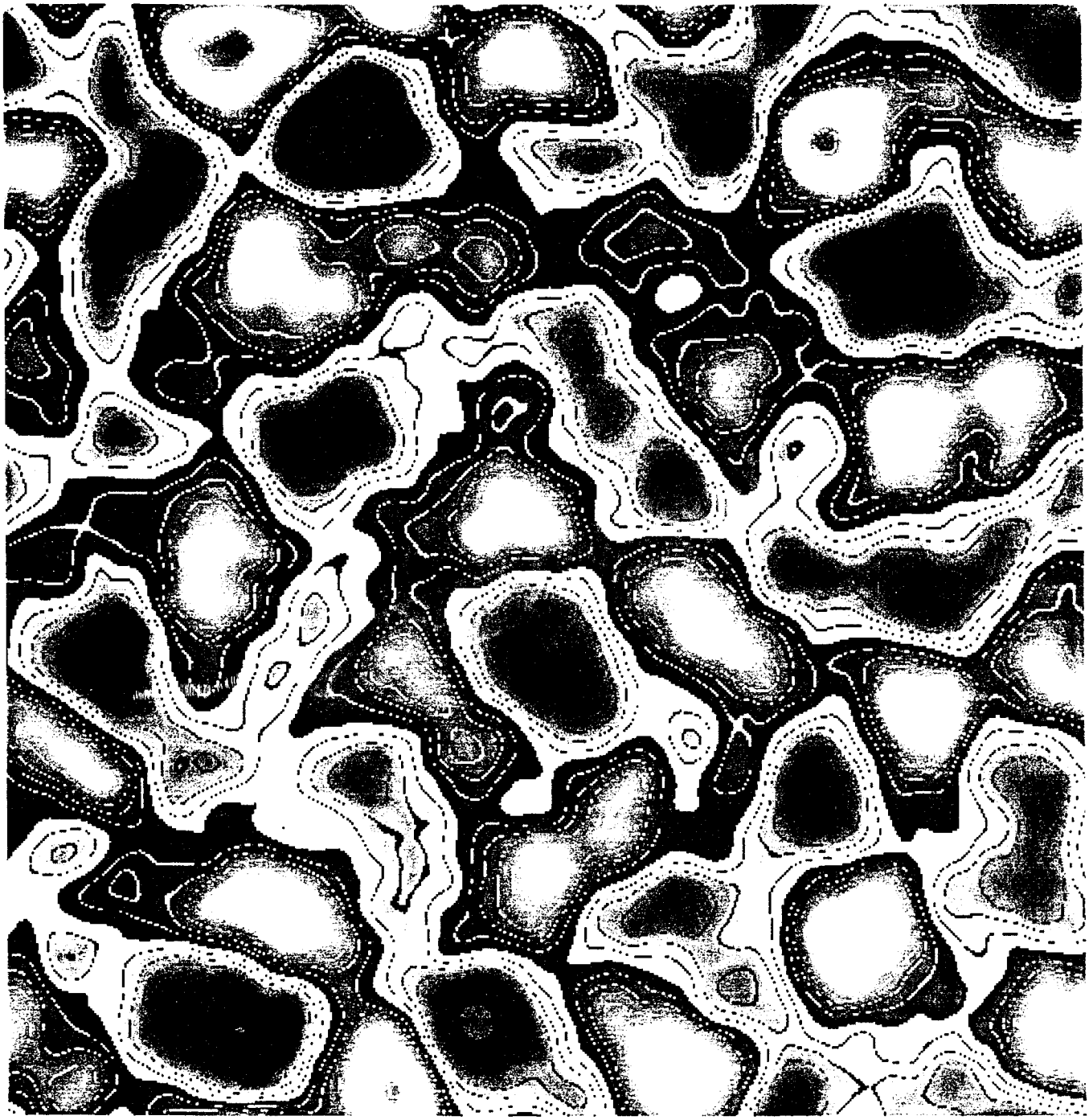

FIG. 1. Equipotential curves in one realization of the electrostatic potential $\Phi(x,y,t=0)$ represented on a spatial grid of 512^2 points for the spectrum $N_0=4$, $N=48$ with the most probable amplitude of energy fluctuations (9%). This is the realization used in the present work. The x axis is horizontal pointing to the right, the y axis is vertical, pointing downward.

by means of the parameters N_0 and N, which also appear as discretization parameters of the problem. In order to represent in a simple way the experimental spectrum which is very wide in frequencies around the diamagnetic drift velocity, we only consider here a single frequency ω. Different phase velocities are associated to the different wave vectors, the large number of which ensures the existence of chaotic trajectories, with positive Lyapunov exponent [8,9]. The appearance of chaos in the systems with three electrostatic waves has been studied in [21,22]; the three-wave system has also been studied recently in [27].

The electrostatic potential (2.2) composed with the above set of isotropic wave vectors can thus be written in the form

$$\Phi(x,y,t)=\frac{a}{2\pi}\sum_{n=-N}^{N}\sum_{m=-N}^{N}\frac{\Theta(n,m;N_0,N)}{(n^2+m^2)^{\alpha/2}} \times\cos\left[\frac{2\pi}{L}(nx+my)+\varphi_{n,m}-\omega t\right] \quad (2.5)$$

in terms of the Heaviside function $\Theta(n,m;N_0,N)$ which is unity for (n,m) values located into the annulus $C(N_0,N)$,

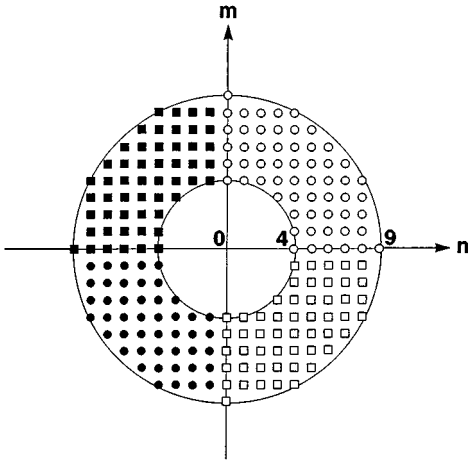

FIG. 2. Simplified example of the wave numbers $n=k_x/k_0$, $m=k_y/k_0$ considered in annulus to represent a discretized spectrum with $N_0=4$ and $N=9$.

and 0 elsewhere. The constant a determines the amplitude of the turbulence. We have introduced here a set of phases $\varphi_{n,m}$ randomly chosen between 0 and 2π. The importance of these random phases will be discussed below. In (2.5) the $k^{-\alpha}$ dependence of the potential can be shown to correspond to a spectral energy density in k^{-I_s} where the value of I_s is given by (see Appendix A)

$$I_s=2\alpha-3. \tag{2.6}$$

In order to describe a k^{-3} spectrum, we thus choose $\alpha=3$. We note that, contrary to the model considered in [19], the amplitudes of the waves in (2.4) describe a realistic k^{-3} spectrum, rather than random amplitudes following an Ornstein-Uhlenbeck process with a prescribed correlation time. Moreover, the number of waves is much more important here (only 64 waves in [19]).

After determining the electrostatic potential associated with the k^{-3} spectrum, we still have to derive analytical expressions for the electric field which drives the particles. The two components of the electric field are easily derived from (2.5):

$$\begin{aligned}\mathbf{E}(x,y,t)&=-\boldsymbol{\nabla}\Phi(x,y,t)\\&=\frac{a}{L}\sum_{n=-N}^{N}\sum_{m=-N}^{N}\binom{n}{m}\frac{\Theta(n,m;N_0,N)}{(n^2+m^2)^{\alpha/2}}\\&\quad\times\sin\left[\frac{2\pi}{L}(nx+my)+\varphi_{n,m}-\omega t\right],\end{aligned} \tag{2.7}$$

where the constant a has still to be expressed in terms of the physical parameters of the problem. From a numerical point of view, in order to save memory, it appears to be interesting [8,9] to split the field (2.7) into static and time-dependent factors:

$$\mathbf{E}(x,y,t)=\mathbf{E}_S(x,y)\cos(\omega t)-\mathbf{E}_C(x,y)\sin(\omega t), \tag{2.8}$$

which vary as $\cos(\omega t)$ and $\sin(\omega t)$, respectively, and can be easily tabulated. The spatial cartographies or maps of the field are

$$\begin{aligned}\mathbf{E}_S(x,y)&=\frac{a}{L}\sum_{n=-N}^{N}\sum_{m=-N}^{N}\binom{n}{m}\frac{\Theta(n,m;N_0,N)}{(n^2+m^2)^{\alpha/2}}\\&\quad\times\sin\left[\frac{2\pi}{L}(nx+my)+\varphi_{n,m}\right],\end{aligned} \tag{2.9}$$

$$\begin{aligned}\mathbf{E}_C(x,y)&=\frac{a}{L}\sum_{n=-N}^{N}\sum_{m=-N}^{N}\binom{n}{m}\frac{\Theta(n,m;N_0,N)}{(n^2+m^2)^{\alpha/2}}\\&\quad\times\cos\left[\frac{2\pi}{L}(nx+my)+\varphi_{n,m}\right].\end{aligned} \tag{2.10}$$

The values of these four scalar functions can be computed once on the $M\times M$ nodes of a spatial grid and kept in memory. These four spatial maps entirely determine one realization of the electric field. The value of M is chosen of the form $M=2^s\gg N$ in such a way as to represent correctly the N smallest wavelengths in the periodic square. The value $M=256$ has been considered in Refs. [8–11]; we will use here $M=512$ (with some numerical checks with $M=1024$) in order to have a good numerical definition of the electric field. The evaluation of the electric field at the exact position of the particle at each time step is performed by using a 16-point interpolation method under a matrix form detailed in Appendix C.

B. Fluctuations of average energy density

In order to relate the amplitude constant a to a physically measurable quantity, we evaluate here the average energy density (per unit volume) defined as

$$\mathcal{E}(t)=\frac{1}{8\pi}\langle E^2(x,y,t)\rangle_{x,y}=\frac{1}{L^2}\int_0^L dx\int_0^L dy\,\frac{1}{8\pi}E^2(x,y,t). \tag{2.11}$$

The result can be decomposed as follows:

$$\begin{aligned}\mathcal{E}(t)&=\frac{1}{8\pi}\left(\frac{a}{L}\right)^2\sigma^2(N,N_0,\alpha)[1+C(\varphi)\cos(2\omega t)\\&\quad+S(\varphi)\sin(2\omega t)].\end{aligned} \tag{2.12}$$

In the square brackets the term unity represents the time average over one period:

$$\langle\mathcal{E}(t)\rangle_\omega=\frac{1}{8\pi}\left(\frac{a}{L}\right)^2\sigma^2(N,N_0,\alpha) \tag{2.13}$$

in terms of the numerical constant

$$\sigma^2(N,N_0,\alpha)=\frac{1}{2}\sum_{n=-N}^{N}\sum_{m=-N}^{N}\frac{\Theta(n,m;N_0,N)}{(n^2+m^2)^{\alpha-1}}, \tag{2.14}$$

which has to be determined numerically in terms of the spectral index α, and of the parameters N and N_0 chosen to represent the discretization of the spectrum, while the other terms in (2.12) represent the temporal modulations $C(\varphi)$ and $S(\varphi)$ in $\sin(2\omega t)$ and $\cos(2\omega t)$,

$$\left.\begin{matrix} C(\varphi) \\ S(\varphi) \end{matrix}\right\} = \frac{1}{\sigma^2}\frac{1}{2}\sum_{n=-N}^{N}\sum_{m=-N}^{N}\frac{\Theta(n,m;N_0,N)}{(n^2+m^2)^{\alpha-1}} \times \left\{\begin{matrix} \cos \\ \sin \end{matrix}\right\}(\varphi_{n,m}+\varphi_{-n,-m}), \tag{2.15}$$

which actually depend on the sum of the random phases. In this problem the choice of a given realization of random phases is found to modify the energy modulations.

Let us evaluate the average properties of these energy modulations in an ensemble of R realizations of the field, i.e., of the random phases. We have

$$\langle \mathcal{E}(t)\rangle_R = \frac{1}{8\pi}\left(\frac{a}{L}\right)^2 \sigma^2[1+\langle C(\varphi)\rangle_R \cos(2\omega t) + \langle S(\varphi)\rangle_R \sin(2\omega t)], \tag{2.16}$$

where the angle brackets denote the ensemble average. We expect that the amplitude of these oscillations should go to zero for a sufficiently large ensemble of realizations: $\lim_{R\to\infty}\langle C(\varphi)\rangle_R = \lim_{R\to\infty}\langle S(\varphi)\rangle_R = 0$. Using the random number generator RANF of the Cray computer we have obtained Gaussian probability functions $P(C)$ and $P(S)$ for both quantities $C(\varphi)$ and $S(\varphi)$, with equal standard deviations $d \simeq 0.09$. We have checked that for $R = 2\times 10^5$ realizations we obtain an average $\langle C(\varphi)\rangle_R \simeq \langle S(\varphi)\rangle_R \simeq 10^{-4}$, while for a larger number of realizations $R = 2\times 10^6$, we obtain indeed a smaller value for the average $\langle C(\varphi)\rangle_R \simeq \langle S(\varphi)\rangle_R \simeq 10^{-5}$. From Eq. (2.12) it is simple to see that the maxima and minima of the time modulations are given by

$$\mathcal{E}_E = \frac{1}{8\pi}\left(\frac{a}{L}\right)^2 \sigma^2(N,N_0,\alpha)[1\pm F(\varphi)], \tag{2.17}$$

where the relative energy fluctuation is simply $F(\varphi) = [C^2(\varphi)+S^2(\varphi)]^{1/2}$. This value has a distribution over an ensemble of realizations, which fits very well with the expected result holding for uncorrelated values of $C(\varphi)$ and $S(\varphi)$ with vanishing averages: the distribution of F is found indeed to be given by $P(F) = 2\pi F P(C)P(S)$ with the most probable value $F_p = d$. This yields roughly 9% of energy modulation in the case $N_0 = 4$, $N = 48$ in which $\sigma^2 = 0.108$. In summary, the choice of one given realization of the random phases to perform trajectory calculations implies a given amplitude $F(\varphi)$ of the energy modulation. The realization could be chosen to be of minimum energy fluctuations ($C \simeq S \simeq F \simeq 0$) but we rather consider here a realization with most probable energy fluctuations ($F \simeq 0.09$).

C. Dimensionless equations of motion

The equation of motion (2.1) for guiding centers takes the following form in the presence of a constant magnetic field in the z direction and an electric field in the perpendicular plane:

$$\frac{d}{dt}\begin{pmatrix} x \\ y \end{pmatrix} = \frac{c}{B}\begin{pmatrix} E_y(x,y,t) \\ -E_x(x,y,t) \end{pmatrix} = \frac{c}{B}\begin{pmatrix} -\nabla_y \Phi(x,y,t) \\ \nabla_x \Phi(x,y,t) \end{pmatrix}. \tag{2.18}$$

These equations describe a nonautonomous Hamiltonian system with one and one-half degrees of freedom. The coordinates x and y are canonically conjugate: the physical space (x,y) is also the phase space of the system. The Hamiltonian is

$$H(x,y,t) = -\frac{c}{B}\Phi(x,y,t). \tag{2.19}$$

From the expressions (2.8)–(2.10) of the electric field, the equation of motion takes the form

$$\frac{d}{dt}\begin{pmatrix} x(t) \\ y(t) \end{pmatrix} = \frac{c}{B}\frac{a}{L}\sum_{n=-N}^{N}\sum_{m=-N}^{N}\begin{pmatrix} m \\ -n \end{pmatrix}\frac{\Theta(n,m;N_0,N)}{(n^2+m^2)^{\alpha/2}} \times \sin\left[\frac{2\pi}{L}(nx+my)+\varphi_{n,m}-\omega t\right]. \tag{2.20}$$

In order to study these equations numerically, we have to use dimensionless variables. Two reasonable choices are possible for reducing spatial units (i) either to the characteristic length L of the periodic square as in Ref. [9], or (ii) to the total number of pixels M along the periodic square: $\overline{x} \equiv Mx/L$, $\overline{y} \equiv My/L$ (which vary from zero to M inside the periodic cell). The unit length is in this case 1 pixel $= L/M = N_0\lambda_{\max}/M = N\lambda_{\min}/M$. We also use $\overline{t} \equiv (\omega/2\pi)t$ and $\overline{\varphi_{n,m}} = (1/2\pi)\varphi_{n,m}$ where the phases $\overline{\varphi}$ are chosen between 0 and 1. In our numerical computations we rather use the latter variables. The equation of motion (2.20) takes the dimensionless form

$$\frac{d}{d\overline{t}}\begin{pmatrix} \overline{x(t)} \\ \overline{y(t)} \end{pmatrix} = 2\pi\beta\begin{pmatrix} \overline{e_y(\mathbf{x},t)} \\ -\overline{e_x(\mathbf{x},t)} \end{pmatrix} = 2\pi\beta\left\{\begin{pmatrix} \overline{e_{y,S}(\mathbf{x})} \\ -\overline{e_{x,S}(\mathbf{x})} \end{pmatrix}\cos(2\pi t) - \begin{pmatrix} \overline{e_{y,C}(\mathbf{x})} \\ -\overline{e_{x,C}(\mathbf{x})} \end{pmatrix}\sin(2\pi t)\right\} \tag{2.21}$$

in which the amplitude β of turbulence is defined by

$$2\pi\beta \equiv \frac{M\mathcal{A}}{\sigma(N,N_0,\alpha)} \tag{2.22}$$

in terms of the constant $\mathcal{A}$:

$$\mathcal{A} \equiv \frac{2\pi}{L}\frac{c}{\omega B}\sqrt{8\pi\langle \mathcal{E}(t)\rangle_\omega} \sim \frac{E}{B}. \tag{2.23}$$

The four spatial functions represent four ''spatial cartographies'' defined by

$$\begin{pmatrix} \overline{e_{y,S}(\mathbf{x})} \\ -\overline{e_{x,S}(\mathbf{x})} \end{pmatrix} = \sum_{n=-N}^{N}\sum_{m=-N}^{N}\begin{pmatrix} m \\ -n \end{pmatrix}\frac{\Theta(n,m;N_0,N)}{(n^2+m^2)^{\alpha/2}} \times \sin\left[2\pi\left(n\,\frac{\overline{x}}{M}+m\,\frac{\overline{y}}{M}+\overline{\varphi_{n,m}}\right)\right], \tag{2.24}$$

$$\begin{pmatrix} \overline{e_{y,C}}(\overline{\mathbf{x}}) \\ -\overline{e_{x,C}}(\overline{\mathbf{x}}) \end{pmatrix} = \sum_{n=-N}^{N} \sum_{m=-N}^{N} \begin{pmatrix} m \\ -n \end{pmatrix} \frac{\Theta(n,m;N_0,N)}{(n^2+m^2)^{\alpha/2}} \times \cos\left[2\pi \left(n \frac{\overline{x}}{M} + m \frac{\overline{y}}{M} + \overline{\varphi_{n,m}} \right) \right]. \tag{2.25}$$

These spatial cartographies are calculated once. The evolution equation (2.21) is solved by a Runge-Kutta algorithm of fourth order. At each time step in the $(j+1)$th period, we have $\overline{t} = j + (1,2,\ldots,p) \times \Delta \overline{t}$, and the right-hand side is evaluated from the values of trigonometric functions of time (which have been tabulated at each time step), and from 16-point spatial interpolations between the nodes of the grid on which the values of the four cartographies (2.24), (2.25) have been memorized: $\overline{\mathbf{x}} \equiv \{r,s\} = (1,2,\ldots,M)$. In the same notations the dimensionless electrostatic potential is (a.u.)

$$\overline{\Phi}(\overline{x},\overline{y},\overline{t}) \simeq \overline{e_{y,C0}}(\overline{\mathbf{x}}) \cos(2\pi\overline{t}) + \overline{e_{y,S0}}(\overline{\mathbf{x}}) \sin(2\pi\overline{t}), \tag{2.26}$$

where we have defined two additional cartographies for the electrostatic potential,

$$\begin{pmatrix} \overline{e_{y,C0}}(\overline{\mathbf{x}}) \\ \overline{e_{y,S0}}(\overline{\mathbf{x}}) \end{pmatrix} = \sum_{n=-N}^{N} \sum_{m=-N}^{N} \frac{\Theta(n,m;N_0,N)}{(n^2+m^2)^{\alpha/2}} \begin{pmatrix} \cos\left[2\pi \left(n \frac{\overline{x}}{M} + m \frac{\overline{y}}{M} + \overline{\varphi_{n,m}} \right) \right] \\ \sin\left[2\pi \left(n \frac{\overline{x}}{M} + m \frac{\overline{y}}{M} + \overline{\varphi_{n,m}} \right) \right] \end{pmatrix}, \tag{2.27}$$

which will be useful to compute the discrete values of these fields by a discrete and complex two-dimensional (2D) fast Fourier transform (FFT) on $M \times M$ points (see Appendix B).

D. Physically measurable parameters

It is important to stress the difference between the discretization parameters (which vary according to the model), and the physical ones (which vary according to the system). The amplitude parameter $\mathcal{A}$ [Eq. (2.23)] actually depends on the length L of the periodic cell; the latter only gets a physical meaning in terms of the wavelengths $\lambda_{\min}$ or $\lambda_{\max}$ by means of the discretization parameters N and N_0 of the model [see Eq. (2.4)]. On the other side, a physical amplitude parameter A should be defined independently of the discretization parameters of the model; since large wavelengths are dominant in the spectrum (small k), we will choose $\lambda_{\max}$ as the reference length to build a nondimensional physical amplitude:

$$A \equiv \frac{2\pi}{\lambda_{\max}} \frac{c}{\omega B} \sqrt{8\pi \langle \mathcal{E}(t) \rangle_{\omega}} = N_0 \mathcal{A} \sim \frac{E}{\omega B}. \tag{2.28}$$

With $N_0 = 4$ the amplitude parameter is thus $A = 4\mathcal{A}$. As far as the amplitude parameter β [Eq. (2.22)] is concerned, it is simply related to the physical amplitude A by the following relation: $A = 2\pi\beta(N_0/M)\sigma(N,N_0,\alpha)$. With $N_0 = 4$, $N = 48$, we find $\sigma = 0.3288$, and with $M = 512$ this yields the relation $\beta = 247.8\mathcal{A}$ or $A = 0.016\,14\beta$.

The diffusion coefficient in physical space is defined, as usual, from the asymptotic limit of the variance of the fluctuating part of the displacement since the initial time $\delta\mathbf{x}(t) \equiv \mathbf{x}(t) - \mathbf{x}(0) - \langle \mathbf{x}(t) - \mathbf{x}(0) \rangle$:

$$D = \lim_{t \to \infty} \frac{\langle \delta \mathbf{x}^2(t) \rangle}{t}. \tag{2.29}$$

This definition coincides with the one used in our previous work [Eq. (16) in Ref. [9]]. It includes the sum of fluctuations in both spatial directions: $\langle \delta\mathbf{x}^2(t) \rangle = \langle \delta x^2(t) \rangle + \langle \delta y^2(t) \rangle$. The average $\langle\ \rangle$ is computed numerically by an average over (64) initial conditions, *and* by a time average over each trajectory (the idea of performing time averages along trajectories, which is usual in statistical mechanics, has been suggested to us by De Leener). The result of the simulation is the numerical diffusion coefficient derived from the equations of motion (2.21):

$$\overline{\mathcal{D}} = \lim_{\overline{t} \to \infty} \frac{\langle \delta\, \overline{\mathbf{x}^2}(\overline{t}) \rangle}{\overline{t}}. \tag{2.30}$$

We determine this quantity by plotting the numerical curve of $\langle \delta\overline{\mathbf{x}^2}(\overline{t}) \rangle$ vs time, up to $t = Q$ (see Fig. 3): the first part of this curve (let us say up to $Q/2$) is generally quite smooth and linear since it represents the average not only on the 64 initial conditions, but also a time average over many intervals of duration t (smaller than $Q/2$) displaced ''like a comb'' along the whole trajectory. These technical points are explained in Sec. III. We determine $\mathcal{D}$ by linear regression in the domain $(0,Q/2)$. The example presented in Fig. 3 corresponds to $A = 160$ and needs for 2.4×10^4 s of CPU time on 64 processors of the Cray T3D computer. The calculation is repeated for several sets of initial conditions, and for different values of A, with different time steps.

The final interpretation of this result consists of calculating a dimensionless coefficient (reduced by means of the characteristic length $\lambda_{\max}$ and time $2\pi/\omega$) by means of

$$\mathbb{D} \equiv \frac{2\pi}{\omega \lambda_{\max}^2} D = N_0^2 \overline{\mathcal{D}} / M^2. \tag{2.31}$$

The aim of the present work consists of determining the exponent γ describing the dependence of the diffusion coefficient

$$\mathbb{D}(A) \equiv \frac{2\pi}{\omega \lambda_{\max}^2} D(A) \simeq A^{\gamma} \tag{2.32}$$

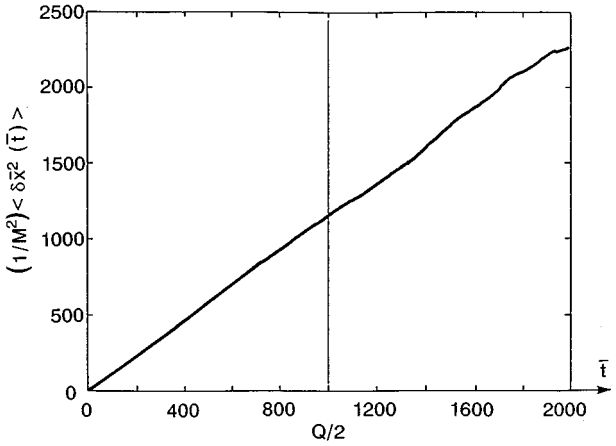

FIG. 3. Example of a diffusion curve $\langle \delta\overline{\mathbf{x}}^2(\overline{t})\rangle$ (in units M^2 or square cells) vs $\overline{t}$ (expressed in periods) up to $t=Q$. Due to the good statistics obtained by the ''comb average,'' the first half of the curve is rather straight and indicates a classical diffusive behavior. The slope of this line is the diffusion coefficient $\mathcal{D}$. Here the amplitude is $A=160$. The number of time steps per period is $N_{\text{step}}=4\times10^4$ resulting in 8×10^7 iterations on each of the 64 particles. Each run lasts between 1 and 17 h on 64 processors of the Cray T3D computer.

as a function of the amplitude parameter A in the low-frequency or high-amplitude regime. From (2.28) the above scaling law implies

$$D(A)\simeq \omega A^{\gamma}\simeq \omega^{1-\gamma}\left(\frac{E}{B}\right)^{\gamma}. \tag{2.33}$$

At low values of the amplitude, we have checked previously that a quasilinear scaling is obtained in numerical simulations [8–10], with $\gamma_{\text{QL}}=2$; an elegant analytical derivation of this expected result has been given for the discrete case in Ref. [28]. This B^{-2} behavior also corresponds to the gyro-Bohm scaling. We have seen in the Introduction that it has been traditionally believed [3,5–7] since the first work by Dupree [3] (based on the truncature by the Corrsin assumption and second cumulant approximation) that the high-amplitude scaling could be a Bohm-like scaling, $\gamma=1$. However, Grusinov, Isichenko, and Kalda [12] have remarked that, in the limit of zero frequency where the Hamiltonian (2.19) becomes time independent, the system reduces to only one degree of freedom, and the diffusion coefficient (2.32) should strictly go to zero. This imposes

$$\xi\equiv 1-\gamma>0, \tag{2.34}$$

i.e., the exponent γ should be strictly smaller than unity, $\gamma<1$. A strict Bohm regime thus appears as impossible in this case. For low frequencies, the percolation prediction [12–15] is $\gamma_I=\frac{7}{10}$ or $\xi_I=\frac{3}{10}$. In Sec. IV we will measure the value of γ by plotting the curve $\ln \mathbb{D}(A)\simeq\gamma\ln(A)$ in logarithmic scale, in a domain of sufficiently large values of the amplitude $A>1$. A similar and related research program is in progress in Brussels, with a different spectrum [29].

III. STRUCTURE OF THE PARALLEL CODE RADIGUET 2

Although the name remains fundamentally the same as in our previous work [10,11], the code RADIGUET 2 is a fully new code for parallel computer Cray T3D. This code involves essentially two parts.

The first part computes the *cartographies* of the potential (2.27) and of the components (2.24), (2.25) of the electric field in a given realization. These results are kept in memory on a spatial grid of $M\times M$ points, with $M=512$; the results have been checked to agree with a more precise grid $M=1024$ and a value $M=256$ is almost sufficient. This program should be used only once in principle, or repeated to obtain different realizations of the fields. This calculation can be performed by a direct summation, or by the complex two-dimensional FFT presented in Appendix B. For a direct calculation with NP processors, we define NP vertical domains in the cartography, to be computed by the various processors. Each processor has to calculate a quadruple loop, one for each component of the wave vector, one for each spatial dimension to be scanned. Then the instructions of the communication library SHMEM allow us to collect these results and build the full cartography on one ''master processor.'' The result is kept in permanent memory in a UNIX file. For more extended cartographies, we have to use a complex FFT of the functions $\tilde{h}_{\lambda,n,m}$ defined in (B8).

The main part of the program is the calculation of the trajectories of $\mathcal{N}$ *particles* ($i=1,2,\ldots,\mathcal{N}$). In all cases, we use $NP=\mathcal{N}$ elementary processors (in general $\mathcal{N}=64$), each one for a different trajectory. In simple cases where the four cartographies of the electric field can be kept in the memory of each processor (8 Mw), it is sufficient to perform each trajectory calculation separately. An individual label is first attributed to each processor, and the four cartographies (2.24), (2.25) of the electric field are charged into the memory. A simple loop evaluates a table of values of $\cos(\tau)$ and $\sin(\tau)$ for the values of $\tau=\omega t$ representing every time step in a period.

A set of $\mathcal{N}$ *initial conditions* $\{x_i(0),y_i(0)\}$ is chosen, equally spaced in the whole elementary cell; each initial condition is introduced in its processing element (PE). The results are actually rather sensitive to this choice: we observe that a slight displacement of the whole set of initial conditions may result in a deviation which can be as large as 10% on the diffusion coefficient. This seems to be the fundamental uncertainty of the results: we thus consider in each realization an ensemble of at least four sets of initial conditions, and repeat the calculation for each one, with different values of the amplitude.

We solve the equations of motion (2.21) over a large number Q of elementary *periods* (2000 or more). The number of *elementary time steps* N_{step} in each period is chosen in such a way as to ensure that the displacement during one time step remains much smaller than the smaller wavelength of the spectrum. The time step has thus to be reduced for large amplitudes where the motion becomes more rapid; we use the condition $N_{\text{step}}=10^3\mathcal{A}$ which is checked to ensure a good convergence of the result. We explore the domain of values of the amplitude $A=4,\ldots,400$. With a spectrum $N_0=4$, $N=48$ this means a domain of values of

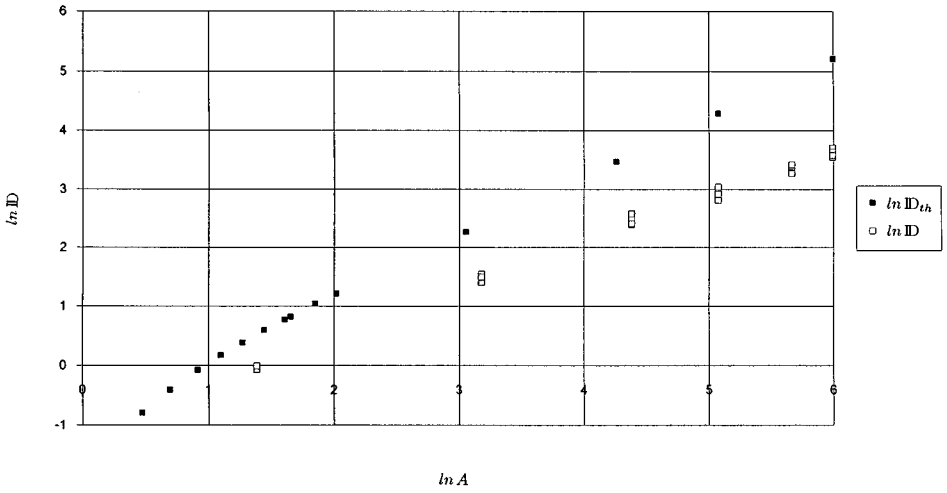

FIG. 4. Reduced diffusion coefficient $\mathbb{D}(A)$ in log-log plot. Black squares represent the Bohm-like theoretical results calculated in Refs. [8,9] from the nonlinear diffusion equation derived in Ref. [7]. Open squares represent the numerical results from the present simulation. The dispersion of the results is obtained by changing slightly the whole set of initial conditions, which results in a possible 10% error on $\mathbb{D}$. This dispersion is used to evaluate the error bar on the slope γ of this curve.

$\mathcal{A}=1,\ldots,100$ and thus values of N_{step} ranging from 10^3 to 10^5 time steps per period.

The *trajectories* $x(\tau)$ and $y(\tau)$ are obtained by solving the equations of motion (2.21) with a fourth-order Runge-Kutta algorithm. It does not seem that a symplectic algorithm would modify the result which consists in the long time behavior of the diffusion coefficient (2.30): the latter is indeed a global statistical quantity involving the average of the mean square displacement over four different sets of 64 initial conditions. The equations of motion are solved every time step inside a double loop: one for every period j and one for every time step k inside each period. After each period j we collect the stroboscopic positions $x_i(j)$ and $y_i(j)$ and we calculate the quadratic displacement of each particle i since the origin of time:

$$r_i^2(j)\equiv[x_i(j)-x_i(0)]^2+[y_i(j)-y_i(0)]^2. \tag{3.1}$$

In order to extract from these trajectories better statistical information, we make use of the stationary property by performing on each trajectory a *time average*. At each period, the present position of the particle can indeed be considered as a new initial position. Thus for each particle i, in its processor, we calculate the time average of (3.1):

$$R_i^2(j)\equiv\frac{1}{Q+1-j}\sum_{l=j}^{Q}\{[x_i(l)-x_i(l-j)]^2 +[y_i(l)-y_i(l-j)]^2\}. \tag{3.2}$$

This amounts to considering a time delay of j periods (let us say a ''*comb*''), and to performing the average over all these intervals defined by displacing the comb of fixed length j from one tooth to the next one, i.e., displacing the initial point from one period to the next one, up to the end of the run ($l=Q$). The final quantity to be evaluated is the *mean square displacement*:

$$\langle\delta\mathbf{x}^2(\tau)\rangle=\langle[\mathbf{x}(\tau)-\mathbf{x}(0)-\langle\mathbf{x}(\tau)-\mathbf{x}(0)\rangle]^2\rangle =\langle[\mathbf{x}(\tau)-\mathbf{x}(0)]^2\rangle-\langle\mathbf{x}(t)-\mathbf{x}(0)\rangle^2, \tag{3.3}$$

where the average over the $\mathcal{N}=64$ trajectories, $\langle\ldots\rangle\equiv1/\mathcal{N}\Sigma_{i=1}^{\mathcal{N}}\cdots$, can only be calculated after collecting all trajectory results on the master processor. The average of the first term in (3.3) is simply the average over trajectories of the expression (3.2). The second term in (3.3) takes into account any possible average motion of the ensemble of particles (barycentric motion); it can also be evaluated by a *comb average* over time; this average involves the following average displacements over the ensemble of particles:

$$X(j)\equiv\frac{1}{\mathcal{N}}\sum_{i=1}^{\mathcal{N}}x_i(j),\quad Y(j)\equiv\frac{1}{\mathcal{N}}\sum_{i=1}^{\mathcal{N}}y_i(j) \tag{3.4}$$

on which a comb average can still be applied. We thus finally evaluate the mean square displacement as follows:

$$W(j)\equiv\langle\delta\,\overline{\mathbf{x}^2}(j)\rangle=\frac{1}{\mathcal{N}}\sum_{i=1}^{\mathcal{N}}R_i^2(j)-\frac{1}{Q+1-j}\times\sum_{l=j}^{Q}\{[X(l)-X(l-j)]^2+[Y(l)-Y(l-j)]^2\} \tag{3.5}$$

by using instruction of the SHMEM library, and keep the results as a function of the discrete time j in a UNIX file.

IV. RESULTS AND DISCUSSION

An example of such a curve is given in Fig. 3. One can see that the first part of the curve (let us say the first half of the total duration of the run, where the statistics is largely better) does not present important oscillations (as observed in the absence of *comb averages*), and appears as rather linear. The diffusion coefficient is computed as the average slope of this first part of the curve, which directly yields a numerical results for the diffusion coefficient (2.30) at a given amplitude.

These calculations are repeated for various initial conditions and for various values of the amplitude β or $\mathcal{A}$. We consider here a realization with the *most probable amplitude of the energy fluctuations* (see Sec. II B). The final plot of numerical results $\ln(\mathbb{D})$ vs $\ln(A)$ [see (2.31), (2.28)] is given in Fig. 4 in the large amplitude domain, and compared with the classical Bohm prediction $\ln(\mathbb{D}_{th})$, as calculated for this spectrum in Ref. [7]. The latter prediction describes a final

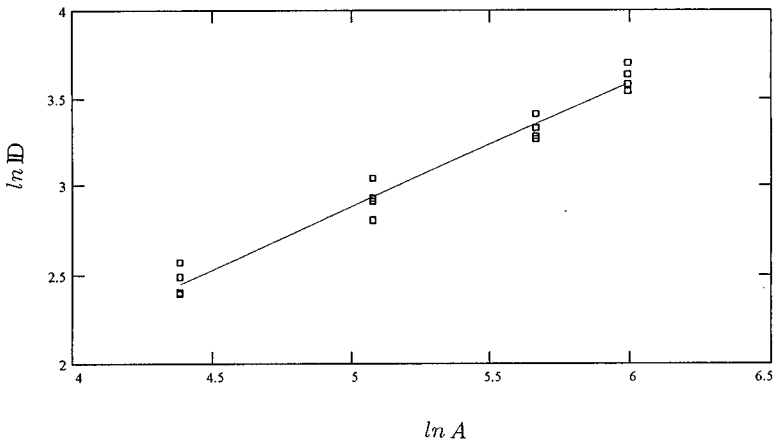

FIG. 5. Result of the linear regression calculation on the 16 numerical results for $\mathbb{D}(A)$ in log-log scale, obtained from the simulation. The resulting straight line has a slope $\gamma=0.704$.

linear increase with a slope $\gamma_B=1$. We observe a deviation of the numerical results from these theoretical predictions and a trend toward an ''asymptotic slope.'' A linear regression or least-squares analysis in the domain of large amplitudes $A=80-400$ yields the final result for the exponent γ defined in (2.32),

$$\gamma=0.704\pm0.030. \tag{4.1}$$

This is the main result of the present paper: this value (4.1) is fully compatible with the Isichenko prediction [12–15] $\gamma_I=\frac{7}{10}$.

The result of the linear regression calculation is shown in Fig. 5. It is worthwhile to make a comment about the evaluation of the error bar in (4.1): it actually represents the mathematical *probable error* [30,31] on the (least-squares) slope of the curve $\ln(\mathbb{D})$ vs $\ln(A)$, computed from the obtained set of points (four points at each value of A: $A=80$, 160, 288, 400), without any interpretation of the data according to the number of particles, etc., as has been performed in [19]. We think it is the most direct evaluation of the error on the slope of a linear regression result; it can be checked that the ensemble of 16 numerical points are correctly inserted inside the bundle of the four straight lines obtained with minimum and maximum values of the two coefficients yielded by the linear regression analysis: this constitutes a graphical test of the validity of the error bar given in (4.1).

In conclusion we see that the spectrum we have considered, with the discretization $N_0=4$, $N=48$, and $M=512$ already allows us to observe the percolation exponent in the domain $A=80-400$, instead of the Bohm exponent $\gamma_B=1$. These are, however, not asymptotically large amplitudes. Moreover, the potential does not seem to involve sufficiently small wavelengths ($\lambda_{\min}/\lambda_{\max}=\frac{1}{12}$) to exhibit fractal equipotential curves as invoked in the Isichenko description. For these reasons we think it necessary to study a much wider spectrum, with a better discretization and thus a much larger number of waves. In order to keep a sufficient description of the smaller wavelengths, the dimension of the spatial grid M should be increased. Of course in order to keep in memory the four cartographies of $M\times M$ points, we have to use the full memory of the 64 processors available for long CPU calculations in the Cray T3D. This program is in progress and we plan to publish the results in the near future.

ACKNOWLEDGMENTS

We want to thank very warmly Professor M. B. Isichenko for several enlightening discussions with one of us (J.H.M.) in the Centre of Physics of Les Houches, for pointing out to us the fundamental inequality (2.34) and suggesting the possibility of using our code to study this problem. We are indebted to Dr. C. Calvin from the Institut National Polytechnique de Grenoble for his valuable aid concerning the parallelization of the two-dimensional complex FFT algorithm. We also thank Professor Michel De Leener from the Université Libre de Bruxelles for his constant interest and for many suggestions originated in our previous common code RADIGUET 1, namely, to use time averages along trajectories and FFT to calculate cartographies. Professor Radu Balescu is also acknowledged for many discussions during a long collaboration on these subjects. Many thanks also to our usual collaborators and friends Boris Weyssow and Eric Vanden Eijnden from the Université Libre de Bruxelles, and Dr. Madalina Vlad and Florin Spineanu from the Institute of Atomic Physics in Bucharest, Romania for several discussions on these points.

APPENDIX A: SPECTRAL INDEX α OF THE DISCRETIZED POTENTIAL

We present here the demonstration of the important relation (2.5) which expresses the index α appearing in the electrostatic model potential (2.4) in terms of the spectral index I_S of the energy density. The latter energy density $\mathcal{E}$ (per unit volume) is written in terms of the spectral energy density $\mathcal{E}_{k_\perp}$ by the same conventional form as in fluid turbulence,

$$\mathcal{E}\simeq\int dk_\perp\mathcal{E}_{k_\perp}\simeq\int d^2k_\perp\,\frac{1}{k_\perp}\,\mathcal{E}_{k_\perp} \tag{A1}$$

and the spectral index I_S is defined by the exponent of the power law $\mathcal{E}_{k_\perp}\sim k_\perp^{-I_S}$. Of course we have

$$\mathcal{E}\simeq\int d^2k_\perp k_\perp^{-(I_S+1)}. \tag{A2}$$

Let us now deduce a similar relation from the expression (2.5) of the model potential, i.e., from

$$\Phi(x,x,t)=\frac{a}{2\pi}\sum_n\sum_m \Phi_{n,m}\cos[\mathbf{k}\cdot\mathbf{x}+\Psi_{\mathbf{k}}(t)], \quad \text{(A3)}$$

where $\mathbf{k}\cdot\mathbf{x}=(2\pi/L)(nx+my)$, $\Psi_{\mathbf{k}}(t)=\varphi_{n,m}-\omega t$, and $\Phi_{n,m}=(n^2+m^2)^{-\alpha/2}\simeq k^{-\alpha}$, in which only the exponent of the wave vector $|k_\perp|\equiv(2\pi/L)(n^2+m^2)^{1/2}$ is of importance for our present purpose. The two components of the electrostatic field $\mathbf{E}=-\boldsymbol{\nabla}\Phi$ can thus be written

$$\mathbf{E}(x,y,t)=\frac{a}{L}\sum_n\sum_m \Phi_{n,m}\begin{pmatrix} n \\ m \end{pmatrix}\sin[\mathbf{k}\cdot\mathbf{x}+\Psi_{\mathbf{k}}(t)]. \quad \text{(A4)}$$

The energy density per unit volume is obtained by averaging over the periodic cell the square of the modulus of the electric field (2.11). From (A4) we immediately see that E^2 introduces $k_\perp^{2-2\alpha}$. By substituting (A4) into (2.11), one deduces the complete result:

$$8\pi\mathcal{E}(t)=\left(\frac{a}{L}\right)^2\sum_n\sum_m \frac{1}{(n^2+m^2)^{\alpha-1}} \times\frac{1}{2}\{1+\cos[\varphi_{\mathbf{k}}+\varphi_{-\mathbf{k}}-2\omega t]\}. \quad \text{(A5)}$$

The announced result (2.6) is deduced after comparing the exponents of $k_\perp$ in the double summation $(1/L^2)\Sigma\Sigma$ of (A5), and in the equivalent double integral in (A2). The comparison yields $I_S+1=2\alpha-2$, thus (2.6). In the particular case of the experimental spectrum $I_S=3$ we have to consider $\alpha=3$ in the discretized potential.

APPENDIX B: DISCRETE AND COMPLEX FFT IN TWO DIMENSIONS

The computation of the various cartographies (2.24), (2.25), (2.27) on a spatial grid of $M\times M$ points can be performed by a direct summation. However, to study several cartographies, or to build more precise cartographies (large number of waves and/or large number of grid points) it becomes necessary to use FFT in 2D. Complex FFT are moreover useful because the sin and cos cartographies appear, by pairs, as the real and imaginary parts of the same transform.

We define as usual the discrete 2D Fourier transform on a grid of $M\times M$ points. Let us consider a periodic function of space

$$f_{r,s}\equiv f(\overline{x=r},\overline{y=s})=\sum_{n_e=0}^{M-1}\sum_{m_e=0}^{M-1}\tilde{f}_{n_e,m_e}e^{i(2\pi/M)(n_e r+m_e s)}, \quad \text{(B1)}$$

which is periodic in $\overline{x=r}$ and in $\overline{y=s}$, with period M. Its discrete and complex FT is

$$\tilde{f}_{n_e,m_e}=\frac{1}{M^2}\sum_{r=0}^{M-1}\sum_{s=0}^{M-1} f_{r,s}e^{-i(2\pi/M)(n_e r+m_e s)}. \quad \text{(B2)}$$

A difficulty comes from the fact that the spatial function (B1) is defined by summations over a square of $M\times M$ ''extended'' values of wave numbers m_e and n_e, while our physical cartographies are defined by summation over a centered annulus of values of n and m. In order to put summations of the type (2.5) in the form (B1), (B2), we split the annulus $C(N_0,N)$ in the (n,m) plane into four parts and reject the four parts at the four inner corners of the extended grid (n_e,m_e) involving $M\times M$ points (see Fig. 6), by means of the following transform:

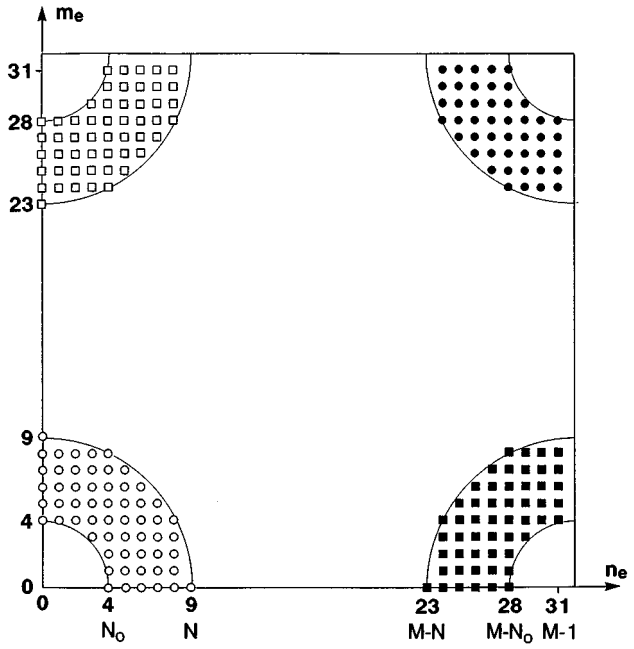

FIG. 6. Extended wave number space (n_e,m_e) to a grid of M^2 points to satisfy FFT requirements. The original annulus describing the spectrum has been split into four parts rejected to the four inner corners of the extended grid. The summation (B7) can be performed from 0 to $M-1$ due to the precise report of the segments $n_e=0$ and $m_e=0$. For clarity we have presented the simplified example $N_0=4$ and $N=9$ as in Fig. 2, and $M=32$.

$$n_e=T_n n\equiv\begin{cases} n & \text{if } n\geq 0 \\ n+M & \text{if } n<0, \end{cases} \quad \text{(B3)}$$

$$m_e=T_m m\equiv\begin{cases} m & \text{if } m\geq 0 \\ m+M & \text{if } m<0. \end{cases} \quad \text{(B4)}$$

We also need the inverse transforms Q_{n_e} and Q_{m_e} used to conserve the amplitude of the waves:

$$n=Q_{n_e}n_e\equiv\begin{cases} n_e-M & \text{if } n_e\geq M/2 \\ n_e & \text{if } n_e<M/2, \end{cases} \quad \text{(B5)}$$

$$m=Q_{m_e}m_e\equiv\begin{cases} m_e-M & \text{if } m_e\geq M/2 \\ m_e & \text{if } m_e<M/2. \end{cases} \quad \text{(B6)}$$

We note that the exact value of n_e or m_e between N and $M-N$ is of no practical importance since all functions on these points will be cut down by the Heaviside function.

By using these transformations in the wave numbers' discrete space, we may transform numerically any summation of an arbitrary function $g(n,m)$ in the small annulus, to an extended summation in the whole $M\times M$ plane:

$$\sum_{n=-N}^{N}\sum_{m=-N}^{N} g(n,m)=\sum_{n_e=0}^{M-1}\sum_{m_e=0}^{M-1} g(Q_{n_e}n_e,Q_{m_e}m_e). \tag{B7}$$

The new Heaviside functions in the extended space are of course zero, except in the four parts of the annulus. In this way we have built formally a periodic function of (n_e,m_e) in the wave number space.

We can now write down the cartographies (2.27) of the potential in a form suitable for discrete FFT, by introducing

$$\begin{pmatrix} \tilde{h}_{\alpha,n,m} \\ \tilde{h}_{\beta,n,m} \\ \tilde{h}_{\gamma,n,m} \end{pmatrix} \equiv \begin{pmatrix} n \\ m \\ 1 \end{pmatrix} \frac{\Theta(n,m;N_0,N)}{(n^2+m^2)^{3/2}}\, e^{i\varphi_{n,m}} \tag{B8}$$

from which we can write (2.27) as

$$\begin{pmatrix} \overline{e_{y,C0}}(\overline{x}=r,\overline{y}=s) \\ \overline{e_{y,S0}}(\overline{x}=r,\overline{y}=s) \end{pmatrix} = \begin{pmatrix} \mathrm{Re} \\ \mathrm{Im} \end{pmatrix} \sum_{n=-N}^{N}\sum_{m=-N}^{N} \tilde{h}_{\gamma,n,m} e^{i(2\pi/M)(nr+ms)} \tag{B9}$$

and from (B7)

$$\begin{pmatrix} \overline{e_{y,C0}}(\overline{x}=r,\overline{y}=s) \\ \overline{e_{y,S0}}(\overline{x}=r,\overline{y}=s) \end{pmatrix} = \begin{pmatrix} \mathrm{Re} \\ \mathrm{Im} \end{pmatrix} \sum_{n=0}^{M-1}\sum_{m=0}^{M-1} \tilde{h}_{\gamma,Qn,Qm} e^{i(2\pi/M)(nr+ms)}, \tag{B10}$$

where we have applied the inverse transform Q to the function $\tilde{h}$. We have also suppressed the subscripts in n_e and m_e, and have taken into account the fact that the exponent is periodic in n of period M so that the transformation does not modify it.

It is simple to see that (2.24) and (2.25) can be written in the same way:

$$\begin{pmatrix} \overline{e_{y,C}}(\overline{x}=r,\overline{y}=s) \\ \overline{e_{y,S}}(\overline{x}=r,\overline{y}=s) \end{pmatrix} = \begin{pmatrix} \mathrm{Re} \\ \mathrm{Im} \end{pmatrix} \sum_{n=0}^{M-1}\sum_{m=0}^{M-1} \tilde{h}_{\beta,Qn,Qm} e^{i(2\pi/M)(nr+ms)}, \tag{B11}$$

$$\begin{pmatrix} \overline{e_{x,C}}(\overline{x}=r,\overline{y}=s) \\ \overline{e_{x,S}}(\overline{x}=r,\overline{y}=s) \end{pmatrix} = \begin{pmatrix} \mathrm{Re} \\ \mathrm{Im} \end{pmatrix} \sum_{n=0}^{M-1}\sum_{m=0}^{M-1} \tilde{h}_{\alpha,Qn,Qm} e^{i(2\pi/M)(nr+ms)}. \tag{B12}$$

These expressions of the two cartographies of the potential (B10) and the four cartographies of the field (B11), (B12) are ready for a discrete complex FFT calculation and therefore for space-discretized evaluation of the space- and time-dependent electrostatic potential and components of the field. The spatial interpolation is detailed in Appendix C.

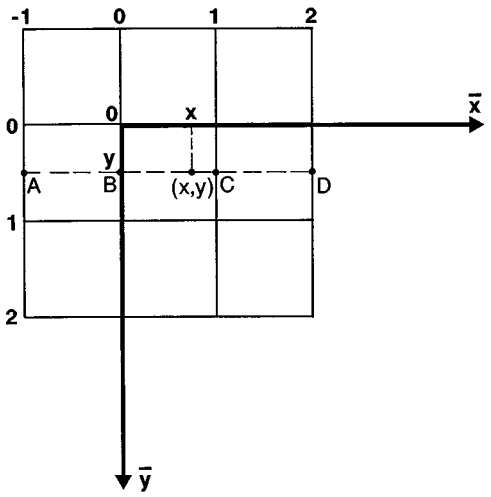

FIG. 7. Orientation of the new axis $O\overline{x}$ and $O\overline{y}$ after translation to the upper left corner of the elementary grid cell containing the position of the particle, i.e., the point where the interpolation has to be performed. This orientation of the axis allows us to make a direct link with the matrix elements $V_{i,j}$ representing the 16 points to be interpolated in the memorized cartography (2.24), (2.25), or (2.27). The first ''vertical'' interpolation (C3) evaluates the field $P_j(y)$ at the points A, B, C, and D for $j=-1,0,1,2$, respectively. The second interpolation (C8) evaluates the field $PP(x,y)$ at the point (x,y).

APPENDIX C: INTERPOLATION WITHIN 16 POINTS ON A GRID

The cartographies (2.24), (2.25), (2.27) are continuous functions $V(x,y)$ of two variables (x,y) from which we keep in memory the sampled values $V_{i,j}$ on a spatial grid (i,j) of $M\times M$ points. At each time step we have to compute these fields at intermediate positions, and we use a 16-point interpolation method described below in two dimensions.

This simple and explicit method is based on Lagrange's classical formula [32] for interpolations of a function of one-variable $P(x)$ between four points $x_1,\ldots,x_4$:

$$\begin{aligned} P(x)=&P(x_1)\frac{(x-x_2)(x-x_3)(x-x_4)}{(x_1-x_2)(x_1-x_3)(x_1-x_4)} \\ &+P(x_2)\frac{(x-x_1)(x-x_3)(x-x_4)}{(x_2-x_1)(x_2-x_3)(x_2-x_4)} \\ &+P(x_3)\frac{(x-x_1)(x-x_2)(x-x_4)}{(x_3-x_1)(x_3-x_2)(x_3-x_4)} \\ &+P(x_4)\frac{(x-x_1)(x-x_2)(x-x_3)}{(x_4-x_1)(x_4-x_2)(x_4-x_3)}. \end{aligned} \tag{C1}$$

This result is generalized here to two dimensions with a simple result in matrix form for interpolations between 16 points on a grid. This set of 4×4 points is displaced on the complete grid of $M\times M$ points $V_{i,j}$ in such a way as to ensure that the unknown point (x,y) is inside the central square. We define the origin $x=0=y$ at the upper left corner of this central square (see Fig. 7). For simplicity we use retrograde axis (x axis pointing to the right, and y axis pointing downwards), which points in the same directions as the matrix indices j and i, respectively. The distance Δx

$=\Delta y \equiv L/M$ between two points on the grid is taken equal to unity here. The known values $V_{i,j}$ on the 16 points are denoted by

$$V_{i,j} \equiv \begin{pmatrix} V_{-1,-1} & V_{-1,0} & V_{-1,1} & V_{-1,2} \\ V_{0,-1} & V_{0,0} & V_{0,1} & V_{0,2} \\ V_{1,-1} & V_{1,0} & V_{1,1} & V_{1,2} \\ V_{2,-1} & V_{2,0} & V_{2,1} & V_{2,2} \end{pmatrix}, \tag{C2}$$

with the convention $i,j=-1,0,1,2$.

First of all we perform a vertical interpolation on each column j, in a point $P_j(y)$ of ordinate $0 \leqslant y \leqslant 1$, i.e., between $V_{0,j}$ and $V_{1,j}$. By using (C1) we find

$$\begin{aligned} P_j(y) &\equiv (P_{-1}(y) \quad P_0(y) \quad P_1(y) \quad P_2(y)) \\ &= C_i(y) V_{i,j} = (C_{-1}(y) \quad C_0(y) \quad C_1(y) \quad C_2(y)) \\ &\times \begin{pmatrix} V_{-1,-1} & V_{-1,0} & V_{-1,1} & V_{-1,2} \\ V_{0,-1} & V_{0,0} & V_{0,1} & V_{0,2} \\ V_{1,-1} & V_{1,0} & V_{1,1} & V_{1,2} \\ V_{2,-1} & V_{2,0} & V_{2,1} & V_{2,2} \end{pmatrix} \end{aligned} \tag{C3}$$

in terms of the known 4×4 matrix and the vector $C_i(y)$ of the four polynomials

$$C_{-1}(z) \equiv -\tfrac{1}{6}z^3 + \tfrac{1}{2}z^2 - \tfrac{1}{3}z, \tag{C4}$$

$$C_0(z) \equiv \tfrac{1}{2}z^3 - z^2 - \tfrac{1}{2}z + 1, \tag{C5}$$

$$C_1(z) \equiv -\tfrac{1}{2}z^3 + \tfrac{1}{2}z^2 + z, \tag{C6}$$

$$C_2(z) \equiv \tfrac{1}{6}z^3 - \tfrac{1}{6}z, \tag{C7}$$

with the obvious and necessary property: $C_{-1}(z)+C_0(z)+C_1(z)+C_2(z)=1$.

Now, from these four values at points of abscissa $x=-1,0,1,2$ and ordinate y, we perform a (horizontal) interpolation on the values of $P_j(y)$ at the point $0 \leqslant x \leqslant 1$ by using the same Lagrange formula (C1). We obtain the interpolated value $PP(x,y)$ at the point (x,y) in the form of a scalar product:

$$PP(x,y) = C_j(x) P_j(y) = C_j(x) C_i(y) V_{i,j}. \tag{C8}$$

More explicitly, we find the interpolated value in the form of a trace of a product of two 4×4 matrices:

$$PP(x,y) = M_{j,i}(x,y) V_{i,j}. \tag{C9}$$

The first one is given by the four known polynomials in x and y,

$$M_{j,i}(x,y) \equiv C_j(x) C_i(y) = \begin{pmatrix} C_{-1}(x)C_{-1}(y) & C_{-1}(x)C_0(y) & C_{-1}(x)C_1(y) & C_{-1}(x)C_2(y) \\ C_0(x)C_{-1}(y) & C_0(x)C_0(y) & C_0(x)C_1(y) & C_0(x)C_2(y) \\ C_1(x)C_{-1}(y) & C_1(x)C_0(y) & C_1(x)C_1(y) & C_1(x)C_2(y) \\ C_2(x)C_{-1}(y) & C_2(x)C_0(y) & C_2(x)C_1(y) & C_2(x)C_2(y) \end{pmatrix}, \tag{C10}$$

and the second matrix in the result (C9) is simply the matrix $V_{i,j}$ of the 16 values surrounding the interpolation point (x,y). This simple and compact result (C9) has not been given explicitly in Ref. [31].

The explicit form of the result (C9) is

$$\begin{aligned} PP(x,y) = {} & C_{-1}(y)\{C_{-1}(x)V_{-1,-1} + C_0(x)V_{-1,0} + C_1(x)V_{-1,1} + C_2(x)V_{-1,2}\} \\ & + C_0(y)\{C_{-1}(x)V_{0,-1} + C_0(x)V_{0,0} + C_1(x)V_{0,1} + C_2(x)V_{0,2}\} \\ & + C_1(y)\{C_{-1}(x)V_{1,-1} + C_0(x)V_{1,0} + C_1(x)V_{1,1} + C_2(x)V_{1,2}\} \\ & + C_2(y)\{C_{-1}(x)V_{2,-1} + C_0(x)V_{2,0} + C_1(x)V_{2,1} + C_2(x)V_{2,2}\}. \end{aligned} \tag{C11}$$

[1] TFR Group and A. Truc, Plasma Phys. Controlled Fusion **26**, 1045 (1984).

[2] P. Liewer, Nucl. Fusion **25**, 543 (1985).

[3] T. H. Dupree, Phys. Fluids **10**, 1049 (1967).

[4] R. Balescu, *Transport Processes in Plasmas* (North-Holland, Amsterdam, 1988), Vol. 2, p. 770.

[5] J. B. Taylor and B. McNamara, Phys. Fluids **14**, 1492 (1971).

[6] D. Montgomery, in *Plasma Physics*, Les Houches. 1972, edited by C. De Witt and J. Peyraud (Gordon and Breach, New York, 1975), p. 427.

[7] J. H. Misguich, R. Balescu, H. L. Pécseli *et al.*, Plasma Phys. Controlled Fusion **29**, 825 (1987).

[8] M. Pettini, A. Vulpiani, J. H. Misguich, R. Balescu, M. De Leener, and J. Orban, Centre d'Etudes de Cadarache EUR-CEA-FC Report No. 1271, 1986 (unpublished).

[9] M. Pettini, A. Vulpiani, J. H. Misguich, R. Balescu, M. De

Leener, and J. Orban, Phys. Rev. A **38**, 344 (1988).
[10] M. De Leener, J. H. Misguich, and R. Balescu, *Second European Theory Meeting*, edited by H. Wilhelmsson, International School of Plasma Physics Pieró Caldirola, Varenna, Italy, 1987, p. 4 (unpublished).
[11] J. H. Misguich, R. Balescu, and R. Nakach, in *Plasma Physics and Controlled Nuclear Fusion Research 1988*, Proceedings of the 12th International Conference on Plasma Physics and Controlled Thermonuclear Fusion, Nice, 1988 (IAEA, Vienna, 1989), p. 521.
[12] A. V. Gruzinov, M. B. Isichenko, and Ya. L. Kalda, Zh. Eksp. Teor. Fiz. **97**, 476 (1990) [Sov. Phys. JETP **70**, 263 (1990)].
[13] M. B. Isichenko and W. Horton, Comments Plasma Phys. Controlled Fusion **14**, 249 (1991).
[14] M. B. Isichenko, Rev. Mod. Phys. **64**, 961 (1992).
[15] M. B. Isichenko, in *Statistical Description of Transport in Plasma, Astro- and Nuclear Physics*, edited by J. H. Misguich, G. Pelletier, and P. Schuck (Nova Science, New York, 1993).
[16] J. H. Misguich and R. Balescu, J. Plasma Phys. **13**, 385 (1975).
[17] S. Corrsin, in *Atmospheric Diffusion and Air Pollution*, edited by F. N. Frenkiel and P. A. Sheppard (Academic, New York, 1990), p. 161.
[18] Hai-Da Wang, M. Vlad, E. Vanden Eijnden, F. Spineanu, J. H. Misguich, and R. Balescu, Phys. Rev. E **51**, 4844 (1995).
[19] M. Ottaviani, Europhys. Lett. **20**, 111 (1992).
[20] G. K. Batchelor, Aust. J. Sci. Res. Ser. A **2**, 437 (1949).
[21] J. H. Misguich and R. Nakach, Phys. Rev. A **44**, 3869 (1991).
[22] G. Petschel and T. Geisel, Phys. Rev. A **44**, 7959 (1991).
[23] C. M. Tchen, H. Pécseli, and S. E. Larsen, Plasma Phys. **22**, 817 (1980).
[24] H. Pécseli, T. Mikkelsen, and S. E. Larsen, Plasma Phys. **25**, 1173 (1983).
[25] P. W. Terry and P. H. Diamond, Phys. Fluids **28**, 1419 (1985).
[26] W. Y. Zhang and R. Balescu, Plasma Phys. Controlled Fusion **29**, 1019 (1987).
[27] B. Weyssow (unpublished).
[28] M. De Leener, Phys. Rev. E **50**, 502 (1994).
[29] B. Weyssow and M. De Leener (unpublished).
[30] H. Margenau and G. M. Murphy, *The Mathematics of Physics and Chemistry* (Van Nostrand, New York, 1956), p. 519.
[31] R. T. Birge, Rev. Mod. Phys. **19**, 298 (1947).
[32] W. H. Press, B. P. Flannery, S. A. Teukolsky, and W. T. Vetterling, *Numerical Recipes* (Cambridge University Press, Cambridge, England, 1987), p. 80.